





ORIGINAL ARTICLE

Artificial intelligence-powered spatial analysis of tumor-infiltrating lymphocytes as a biomarker in locally advanced unresectable thymic epithelial neoplasm: A single-center, retrospective, longitudinal cohort study

Dong Hyun Kim¹  | Yoojoo Lim² | Sukjun Kim² | Chan-Young Ock² | Jeonghwan Youk^{1,3} | Miso Kim^{1,3} | Tae Min Kim^{1,3} | Dong-Wan Kim^{1,3}  | Hak Jae Kim⁴  | Jiwon Koh⁵ | Kyeong Cheon Jung⁵ | Kwon Joong Na⁶ | Chang Hyun Kang⁶ | Bhumsuk Keam^{1,3} 

¹Department of Internal Medicine, Seoul National University Hospital, Seoul, Republic of Korea

²Lunit, Seoul, Republic of Korea

³Cancer Research Institute, Seoul National University College of Medicine, Seoul, Republic of Korea

⁴Department of Radiation Oncology, Seoul National University Hospital, Seoul, Republic of Korea

⁵Department of Pathology, Seoul National University Hospital, Seoul, Republic of Korea

⁶Department of Thoracic and Cardiovascular Surgery, Seoul National University Hospital, Seoul, Republic of Korea

Correspondence

Bhumsuk Keam, Department of Internal Medicine, Seoul National University Hospital, 101, Daehak-ro, Jongro-gu, Seoul 03080, Republic of Korea.
Email: bhumsuk@snu.ac.kr

Abstract

Background: Thymic epithelial tumors (TET) are rare malignancies and lack well-defined biomarkers for neoadjuvant therapy. This study aimed to evaluate the clinical utility of artificial intelligence (AI)-powered tumor-infiltrating lymphocyte (TIL) analysis in TET.

Methods: Patients initially diagnosed with unresectable thymoma or thymic carcinoma who underwent neoadjuvant therapy between January 2004 and December 2021 formed our study population. Hematoxylin and eosin-stained sections from the initial biopsy and surgery were analyzed using an AI-powered spatial TIL analyzer. Intratumoral TIL (iTIL) and stromal TIL (sTIL) were quantified and their immune phenotype (IP) was identified.

Results: Thirty-five patients were included in this study. The proportion of patients with partial response to neoadjuvant therapy was higher in the group with nondesert IP in preneoadjuvant biopsy (63.6% vs. 17.6%, $p = 0.038$). A significant increase in both iTIL (median 22.18/mm² vs. 340.69/mm², $p < 0.001$) and sTIL (median 175.19/mm² vs. 531.02/mm², $p = 0.004$) was observed after neoadjuvant therapy. Patients with higher iTIL (>147/mm²) exhibited longer disease-free survival (median, 29 months vs. 12 months, $p = 0.009$) and overall survival (OS) (median, 62 months vs. 45 months, $p = 0.002$). Patients with higher sTIL (>232.1/mm²) exhibited longer OS (median 62 months vs. 30 months, $p = 0.021$).

Conclusions: Nondesert IP in initial biopsy was associated with a better response to neoadjuvant therapy. Increased infiltration of both iTIL and sTIL in surgical specimens were associated with longer OS in patients with TET who underwent resection followed by neoadjuvant therapy.

KEYWORDS

artificial intelligence-analysis, thymic epithelial tumor, tumor-infiltrating lymphocyte

INTRODUCTION

Complete surgical resection is the only potentially curative treatment for thymic epithelial tumors (TET).^{1–3} Therefore, complete resection is the treatment goal in patients without systemic and/or extra thoracic metastasis. However, even in the absence of distant metastasis, surgery is often difficult due to abutment or local invasion of nearby structures, such as the great vessels.⁴ Consequently, complete resection is not always possible, which results in a high risk of relapse.⁵ Therefore, for patients with locally advanced or advanced-stage TET, in whom imaging studies reveal poor possibility of complete resection of tumors, a curative-intent sequential strategy is recommended in the order of initial needle biopsy, neoadjuvant therapy, and surgery.^{6–8} Given the sensitivity of TETs to platinum-based chemotherapy (CTx), cisplatin-based combination regimens can be used as neoadjuvant therapy.^{9–11} Moreover, as TETs are sensitive to radiotherapy, neoadjuvant concomitant chemoradiotherapy (CCRT) is also a viable option.^{12,13}

However, TET is rare, and there is no established standard treatment for neoadjuvant therapy.¹⁴ Similarly, there is limited evidence regarding the use of adjuvant CTx or CCRT for R1 or R2 resections after surgery. Therefore, we report our experience with 35 patients with TET who received neoadjuvant CTx or CCRT due to the advanced stage at the time of initial diagnosis, with the aim of evaluating the response rate and efficacy of neoadjuvant therapy. Furthermore, since the primary objective of neoadjuvant therapy is to enhance the likelihood of complete resection, the response rate is important. Thus, we evaluated the paired pathology specimens consisting of a preneoadjuvant therapy sample and a surgical sample using an artificial intelligence (AI)-powered tumor-infiltrating lymphocyte (TIL) analyzer (Lunit SCOPE IO).¹⁵ We hypothesized that TIL density or immune phenotype (IP) determined by TIL may predict response to neoadjuvant therapy in advanced TET and possibly related to survival outcomes.

METHODS

Study participants and design

This single-center, retrospective, longitudinal cohort study included patients with TET who underwent curative-intent neoadjuvant CTx or CCRT between January 2004 and December 2021. Patients initially diagnosed with unresectable thymoma (TM) or thymic carcinoma (TC) who underwent neoadjuvant therapy were included in this study. The treatment modality was determined by a multidisciplinary team. The most effective treatment modality is yet to be established, and therefore a multidisciplinary approach, including surgery, CTx, and radiotherapy, is required.

A total of 35 patients who met the inclusion criteria were identified from the database. Their electronic medical records were reviewed for demographics and factors related to diagnosis including stage, response to neoadjuvant therapy,

factors related to surgery, and survival outcomes. Responses were evaluated using RECIST 1.1.¹⁶ All preneoadjuvant therapy and surgical specimens were reviewed by two independent pathologists (JK and KCJ), and the surgical specimens were scored for tumor response grade (TRG).^{17,18}

The analysis was conducted in two steps. The first step evaluated the relationship between TIL density or IP of preneoadjuvant therapy specimens, that is, initial needle biopsy specimens at diagnosis, and response to neoadjuvant therapy. In this analysis, only the patients with hematoxylin and eosin (H&E)-stained archival tumor tissues were included. Second, we analyzed the association between TIL density or IP in surgical specimens and survival outcomes. Since there were several H&E-stained sections per patient, the slide with the largest cancer area was analyzed as the representative slide for that patient. TIL density was obtained by analyzing the H&E-stained sections of patients using Lunit SCOPE IO. Figure 1 illustrates the cohort assembly strategy.

This study was conducted in accordance with the Declaration of Helsinki and the Good Clinical Practice guidelines. The study protocol was approved by the Institutional Review Board of Seoul National University Hospital (IRB no. H-2201-005-1285). The need for informed consent was waived due to the retrospective nature of the study.

Study procedures

Lunit SCOPE IO (Lunit Inc., Seoul, Republic of Korea) is an AI-powered spatial TIL analyzer that identifies and quantifies TIL within the cancer epithelium (intratumoral TIL; iTIL) and stroma (stromal TIL; sTIL) in H&E-stained whole-slide images (WSI). It is composed of two convolutional neural networks, one of which performs segmentation of the cancer area (CA) and cancer-related stroma (CS), and the other identifies TILs. Lunit SCOPE IO was originally trained and optimized using $2.8 \times 10^9 \mu\text{m}^2$ of H&E-stained tissue regions containing 6.0×10^5 TILs, extracted from 3166 WSI assorted from 25 different tumor types, and annotated by board-certified pathologists.¹⁵ The model used in this study was updated via further training and optimization using $1.4 \times 10^{10} \mu\text{m}^2$ of CA and CS, including 6.23×10^5 TILs, extracted from 18 679 H&E-stained WSI of 17 different solid tumor types including thymic origin.

In this study, Lunit SCOPE IO segmented WSI into CA and CS, and separately identified and quantified TIL in each area. The model then estimated the densities of iTIL or sTIL per 1 mm^2 of the corresponding tissue area in each case. Moreover, the model used the densities of iTILs and sTILs in 0.25 mm^2 -sized grids to derive IP of each grid: inflamed-grids having iTIL density of $\geq 130/\text{mm}^2$; immune-excluded-grids having sTIL density of $\geq 260/\text{mm}^2$ and iTIL density of $< 130/\text{mm}^2$; and immune-desert—grids having iTIL and sTIL densities of $< 130/\text{mm}^2$ and $< 260/\text{mm}^2$, respectively. The inflamed score (IS), immune-excluded score (IES), and immune-desert score (IDS) of the WSI were defined as the number of grids annotated to a certain IP divided by the total number of grids analyzed in the WSI. Finally, the representative IP for each

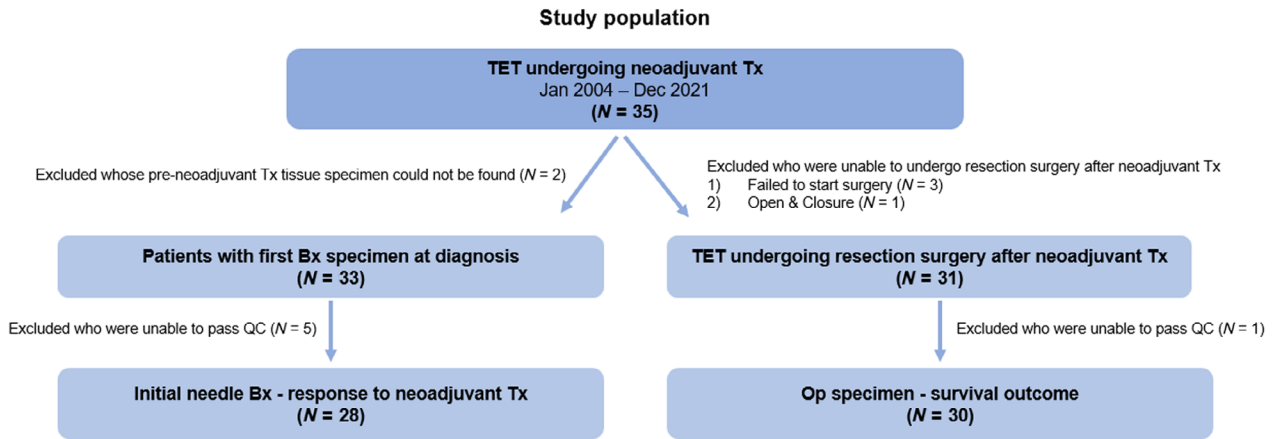


FIGURE 1 Details of cohort assembly strategy.

TABLE 1 Baseline characteristics.

	All patients <i>N</i> = 35	TC <i>N</i> = 28	TM <i>N</i> = 7	<i>p</i> -value
Age, year, median (range)	56 (34–73)	56 (37–73)	51 (34–66)	0.253
Sex, male, <i>n</i> (%)	25 (71.4)	21 (75.0)	4 (57.1)	0.640
Diabetes mellitus, <i>n</i> (%)	4 (11.4)	4 (14.3)	0 (0.0)	0.690
Preoperative symptom, <i>n</i> (%)				
Chest discomfort	9 (25.7)	7 (25.0)	2 (28.6)	1.000
Chest pain	10 (28.6)	9 (32.1)	1 (14.3)	0.640
Hoarseness	8 (22.9)	6 (21.4)	2 (28.6)	1.000
Facial edema	4 (11.4)	4 (14.3)	0 (0.0)	0.690
None	11 (31.4)	7 (25.0)	4 (57.1)	0.237
Histological type, TC, <i>n</i> (%)				
Well differentiated, squamous-cell		14 (50.0)		
Poorly differentiated, squamous-cell		11 (39.3)		
Others		3 (10.7)		
Histological type, TM, <i>n</i> (%)				
B1			3 (42.9)	
B3			4 (57.1)	
Clinical tumor size, cm, median (range)	7.5 (3–12.9)	7.3 (3–9.8)	7.5 (5.9–12.9)	0.135
Clinical TNM staging, <i>n</i> (%)				0.219
III	17 (48.6)	13 (46.4)	4 (57.1)	
IV	18 (51.4)	15 (53.6)	3 (42.9)	
Neoadjuvant therapy, <i>n</i> (%)				0.546
Chemotherapy	5 (14.3)	5 (17.9)	0 (0.0)	
Concurrent chemoradiotherapy	30 (85.7)	23 (82.1)	7 (100.0)	
Response to neoadjuvant therapy, <i>n</i> (%)				0.445
Partial response	13 (37.1)	9 (32.1)	4 (57.1)	
Stable disease	21 (60.0)	18 (64.3)	3 (42.9)	
Progressive disease	1 (2.9)	1 (3.6)	0 (0.0)	

Abbreviations: TC, thymic carcinoma; TM, thymoma.

WSI was defined as inflamed IP if the IS was $\geq 20.0\%$, immune-excluded IP if the IES was $\geq 33.3\%$ and IS was $< 20.0\%$, or immune-desert IP otherwise. The TIL and IS threshold to determine the grid- and WSI-level IP classification

was determined prior to the study as the threshold that optimally predicted high interferon- γ -responsive gene signature levels in a set of TCGA pan-carcinoma tumor samples ($N = 7454$).^{19,20}

TABLE 2 Preneoadjuvant specimen analysis using Lunit SCOPE IO.

Preneoadjuvant specimen	N = 28
Intratumoral TIL density (/mm ²), median (range)	22.18 (0–1870.43)
Stromal TIL density (/mm ²), median (range)	163.56 (1.62–865.51)
Immune phenotype, n (%)	
Inflamed	5 (17.9)
Immune-excluded	6 (21.4)
Immune desert	17 (60.7)

Abbreviation: TIL, tumor-infiltrating lymphocyte.

Statistical analysis

Categorical variables were compared between the two groups using Fisher's exact test or Chi-square test, and *p*-values were two-sided. Differences in the means or medians of the continuous variables between the two groups were assessed using the Wilcoxon rank-sum test. Multivariable logistic regression models were created to identify independent associations with response to neoadjuvant therapy. The cutoff for differentiating between low and high TIL was defined as the point with the lowest *p*-value for overall survival (OS) using the log-rank test for all possible levels for

	All patients N = 28	Desert N = 17	Nondesert N = 11	<i>p</i> -value
Age, year, median (range)	56 (37–73)	51 (37–71)	60 (39–73)	0.140
Sex, male, n (%)	19 (67.9)	12 (70.6)	7 (63.6)	1.000
Diagnosis, n (%)				0.305
Thymic carcinoma	24 (85.7)	16 (94.1)	8 (72.7)	
Thymoma	4 (14.3)	1 (5.9)	3 (27.3)	
Clinical TNM staging, n (%)				1.000
III	15 (53.6)	9 (52.9)	6 (54.5)	
IV	13 (46.4)	8 (47.1)	5 (45.5)	
Neoadjuvant therapy, n (%)				0.588
Chemotherapy	5 (17.9)	2 (11.8)	3 (27.3)	
Concurrent chemoradiotherapy	23 (82.1)	15 (88.2)	8 (82.7)	
Response to neoadjuvant therapy, n (%)				0.038
Partial response	10 (35.7)	3 (17.6)	7 (63.6)	
Stable disease	18 (64.3)	14 (82.4)	4 (36.4)	

Abbreviations: IP, immune phenotype.

TABLE 3 Comparison between desert and nondesert IP of preneoadjuvant therapy.

	Univariable		Multivariable	
	OR (95% CI)	<i>p</i> -value	OR (95% CI)	<i>p</i> -value
Age, years	1.05 (0.97–1.14)	0.2399	1.06 (0.95–1.18)	0.3288
Sex				
Female	1		1	
Male	1.17 (0.22–6.2)	0.5247	1.13 (0.11–11.36)	0.9174
Diagnosis				
Thymic carcinoma	1		1	
Thymoma	2.0 (0.24–16.93)	0.5247	0.75 (0.03–19.67)	0.8610
Clinical TNM staging				
III	1		1	
IV	1.25 (0.27–5.89)	0.7777	4.46 (0.35–56.53)	0.2488
Neoadjuvant therapy				
Concurrent chemoradiotherapy	1		1	
Chemotherapy	0.39 (0.04–4.06)	0.4301	0.02 (0.00–1.45)	0.0750
IP of preneoadjuvant specimen				
Nondesert	1		1	
Desert	0.12 (0.02–0.70)	0.0187	0.04 (0.00–0.77)	0.0325

Abbreviations: CI, confidence interval; IP, immune phenotype; OR, odds ratio.

TABLE 4 Univariable and multivariable analysis.

TABLE 5 Operative outcome.

	N = 30
Age, year, median (range)	56 (34–73)
Sex, male, <i>n</i> (%)	20 (66.7)
Diagnosis, thymic carcinoma, <i>n</i> (%)	23 (76.7)
Time between surgery and end of neoadjuvant therapy, day, median (range)	44 (10–130)
Thymectomy type, <i>n</i> (%)	
Total thymectomy	28 (93.3)
Partial thymectomy	2 (6.7)
Resected structures, <i>n</i> (%)	
Lung	22 (73.3)
Diaphragm	14 (46.7)
Pericardium	25 (83.3)
Innominate vein	23 (76.7)
Phrenic nerve	12 (40.0)
Complete resection, <i>n</i> (%)	25 (83.3)
Pathological Masaoka-Koga stage, <i>n</i> (%)	
Pathological CR	1 (3.3)
I	0 (0.0)
II	7 (23.3)
III	15 (50.0)
VI	7 (23.3)
Pathological TNM stage, <i>n</i> (%)	
Pathological CR	1 (3.3)
I	7 (23.3)
II	3 (10.0)
III	12 (40.0)
VI	7 (23.3)
TRG score, <i>n</i> (%)	
1	1 (3.3)
2	6 (20.0)
3	10 (33.3)
4	12 (40.0)
5	1 (3.3)
Adjuvant treatment, <i>n</i> (%)	
None	18 (60.0)
Chemotherapy	7 (23.3)
Radiotherapy	4 (14.4)
Concurrent chemoradiotherapy	1 (3.3)
Surgical specimen analyzed by Lunit SCOPE IO	
	N = 30
Intratumoral TIL density (/mm ²), median (range)	374.99 (5.79–7415.21)
Stromal TIL density (/mm ²), median (range)	531.02 (96.75–1729.08)
Immune phenotype score (%), median (range)	
Inflamed	37.7 (0.3–94.5)
Immune-excluded	18.5 (0.0–58.8)
Immune desert	32.2 (2.3–96.1)

(Continues)

TABLE 5 (Continued)

Surgical specimen analyzed by Lunit SCOPE IO		N = 30
Immune phenotype, <i>n</i> (%)		
Inflamed		20 (66.7)
Immune-excluded		2 (6.7)
Immune desert		8 (26.7)

Abbreviations: CR, complete response; TIL, tumor-infiltrating lymphocyte; TRG, tumor regression grade.

each biomarker. The Kaplan–Meier method was used to estimate disease-free survival (DFS) and OS. The log-rank test was used to assess the differences between the groups in terms of DFS and OS. The statistical software “R” version 4.1.3 (www.r-project.org) was used for all statistical analyses. *p*-values of <0.05 were considered statistically significant.

RESULTS

Patient and disease characteristics

The baseline characteristics of the 35 patients are presented in Table 1. A total of 30 patients received CCRT as neoadjuvant therapy with weekly cisplatin (median cycle, 5) and a median radiation dose of 44 Gy. The remaining five patients were treated with CTx; four with cisplatin, doxorubicin, and cyclophosphamide; and one with cisplatin and etoposide. Overall, the response to neoadjuvant therapy was partial response (PR) in 13 (37.1%) patients, stable disease (SD) in 21 (60.0%) patients, and progressive disease (PD) in 1 (2.9%) patient.

IP of preneoadjuvant therapy specimen

A total of 33 of 35 patients had preneoadjuvant therapy H&E slides and were evaluated using the Lunit SCOPE IO. The specimens of five patients did not pass quality control, resulting in 28 patients being included in this analysis. The results of the analysis using the Lunit SCOPE IO are presented in Table 2. The median iTIL and sTIL densities in the 28 patients were 22.18/mm² (interquartile range [IQR], 5.37–52.42) and 163.56/mm² (IQR, 42.32–385.55), respectively. More than 60% (17 of 28) of the patients had immune-desert IP, whereas only five (17.9%) had inflamed IP.

We compared the patients with desert and nondesert IP (Table 3). No differences were observed between the two groups in terms of demographics or disease characteristics. However, the proportion of patients with PR to neoadjuvant therapy was higher in the nondesert group (63.6% vs. 17.6% for nondesert vs. desert, respectively, *p* = 0.038).

Table 4 shows the factors associated with response to neoadjuvant therapy. Univariate analysis revealed that the

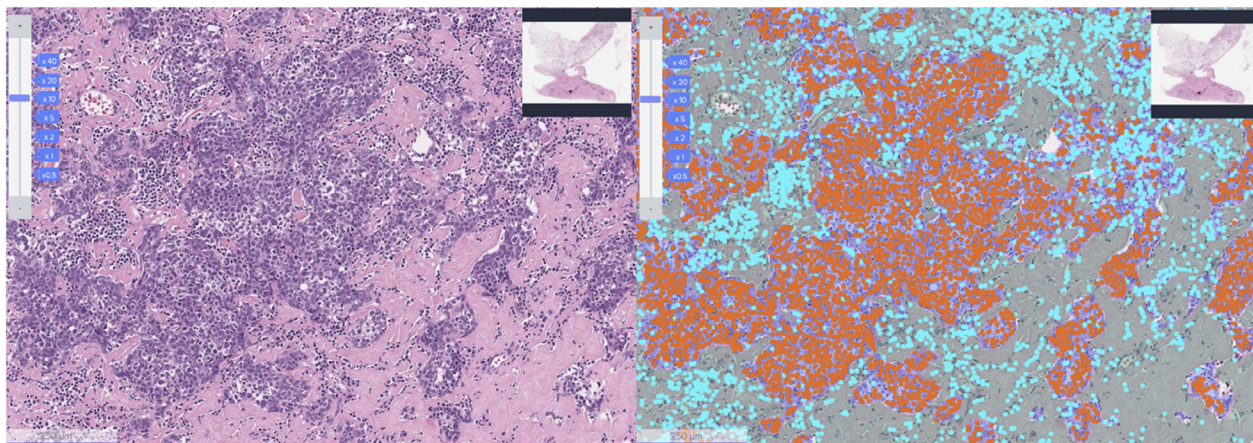


FIGURE 2 Representative image of Lunit SCOPE IO. Representative image of hematoxylin and eosin (H&E) original image (left) and Lunit SCOPE IO-inferred segmentation of cancer epithelium (orange), cancer stroma (grass green), and TIL (cyan blue), respectively (right).

desert IP of preneoadjuvant specimens was associated with response to neoadjuvant therapy. In multivariable analysis, only desert IP of preneoadjuvant specimen (odds ratio [OR] = 0.04, 95% confidence interval [CI]: 0.00–0.77; $p = 0.0325$) was associated with PR. CTx alone as neoadjuvant therapy seemed to reduce the probability of PR; however, the difference was not statistically significant ($p = 0.588$).

Operative outcomes

A total of 31 of 35 patients underwent resection surgery, and the H&E slides of their surgical specimens were evaluated using Lunit SCOPE IO. The sample of one patient did not pass quality control, resulting in 30 patients being included in the analysis. Table 5 shows the operative outcomes. A total of 28 of 30 patients underwent total thymectomy, and complete resection was achieved in 25 (83.3%). TNM staging revealed that pathological complete response (pCR) was observed in one patient and tumor downstaging occurred in 18 (60%). The need for and method of adjuvant therapy was determined by a multidisciplinary team based on the pathology results and clinical situation. A total of 18 (60%) patients received no adjuvant therapy, seven (23.3%) received CTx, four (14.4%) received radiotherapy, and one (3.3%) received CCRT.

Surgical specimen analysis using Lunit SCOPE IO

The results of the analysis of the surgical specimens using Lunit SCOPE IO are presented in Figure 2 and Table 5. The median iTIL and sTIL densities in the 30 patients were $374.99/\text{mm}^2$ (IQR, 126.77–1166.61) and $531.02/\text{mm}^2$ (IQR, 233.84–928.04), respectively. The IP of each 1 mm^2 grid was determined for spatial analysis of TIL distribution. The

median IS, IES, and IDS in this cohort were 37.7, 18.5, and 32.2%, respectively. In contrast to preneoadjuvant specimens, more than 60% (20 of 30) of the patients had inflamed IP, whereas only eight (26.7%) had immune-desert IP.

To examine the changes in TIL density before and after neoadjuvant therapy, we analyzed 28 patients whose pre- and post-neoadjuvant samples were available and passed quality control in the Lunit SCOPE IO analysis. In TET, a significant increase in both iTIL (median $22.18/\text{mm}^2$ vs. $340.69/\text{mm}^2$, $p < 0.001$) and sTIL (median $175.19/\text{mm}^2$ vs. $531.02/\text{mm}^2$, $p = 0.004$) was observed after neoadjuvant therapy. The difference between needle biopsy and surgery resulted in a larger cancer area in the surgical specimens; however, there was no correlation between greater TIL density and cancer area.

Post-neoadjuvant TIL density and survival outcomes

The 5-year OS rate was 73.8% (95% CI: 55.4%–98.2%), with a median follow-up of 41 months. The median OS was 62 months (Figure 3a, 95% CI: 62 months–not reached). The 3-year DFS rate was 29.3% (95% CI: 14.9%–57.4%). The median DFS was 23 months (Figure 3b, 95% CI: 13 months–not determined). The optimal cutoff thresholds for high and low iTIL and sTIL densities were determined to be $147/\text{mm}^2$ and $232.1/\text{mm}^2$, respectively, using the log-rank test. Using this threshold, 22 (73.3%) and 23 (76.7%) patients were categorized in the high iTIL and high sTIL groups, respectively. Patients with higher iTIL density ($>147/\text{mm}^2$) exhibited longer OS (Figure 4a, median OS 62 vs. 45 months, $p = 0.002$) and DFS (Figure 4b, median DFS 29 months vs. 12 months, $p = 0.009$). Patients with higher sTIL density ($>232.1/\text{mm}^2$) exhibited longer OS (Figure 4c, median OS 62 months vs. 30 months, $p = 0.021$). Contrary to iTIL, the higher sTIL density

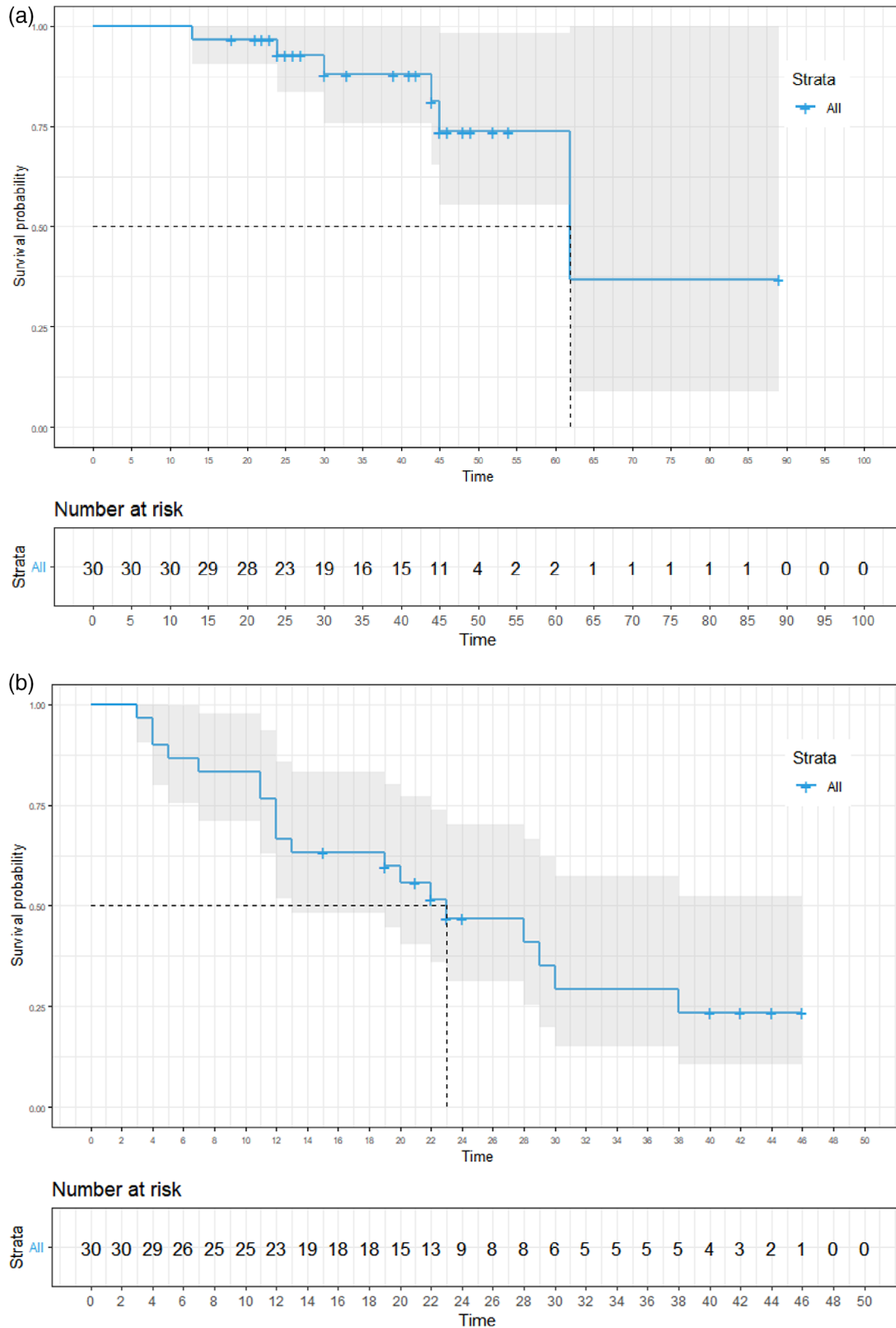


FIGURE 3 Survival outcomes. (a) Kaplan–Meier curves of overall survival (OS). (b) Kaplan–Meier curves of disease-free survival (DFS).

group was not significantly superior to the lower sTIL density group in terms of DFS (Figure 4d, median DFS 28 months vs. 20 months, $p = 0.41$).

To clarify whether the IP of post-neoadjuvant therapy would also serve as a prognostic biomarker for TET-like TIL density, we analyzed the survival outcomes according to

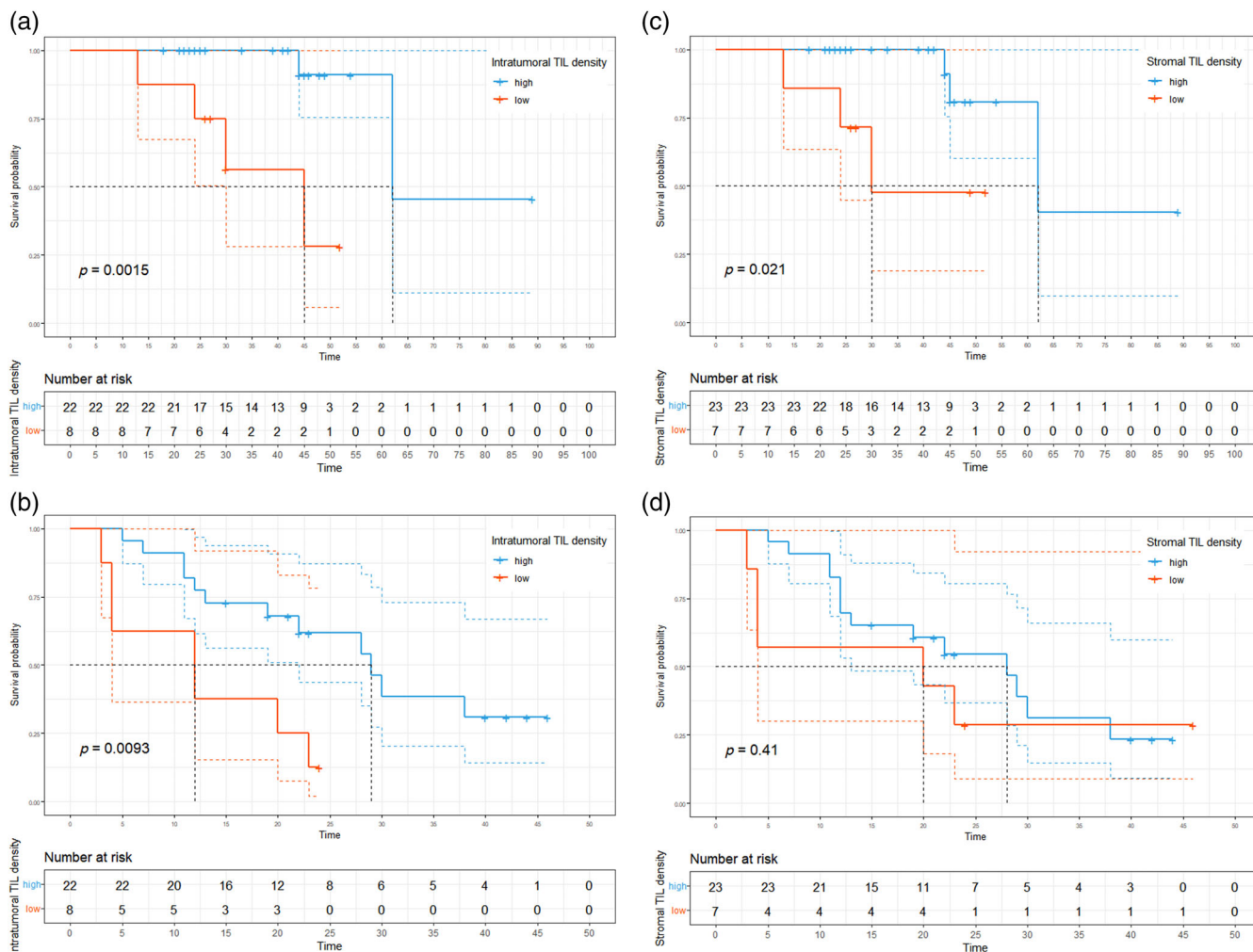


FIGURE 4 Survival outcomes based on tumor-infiltrating lymphocytes (TIL) density. (a) Kaplan–Meier curves of overall survival (OS) based on intratumoral TIL density. (b) Kaplan–Meier curves of disease-free survival (DFS) based on intratumoral TIL density. (c) Kaplan–Meier curves of overall survival (OS) based on stromal TIL density. (d) Kaplan–Meier curves of disease-free survival (DFS) based on stromal TIL density.

IP. No significant differences were observed between patients with desert and nondesert IPs in terms of OS and DFS. The median OS was not determined (95% CI: 30 months not determined) in patients with desert IP. On the other hand, the median OS was 62 months (95% CI: 62 months not determined) in patients with nondesert IP (Figure 5a, $p = 0.32$). The median DFS was 21.5 months (95% CI: 12 months–not determined) in patients with desert IP and 28 months (95% CI: 13 months–not determined) in patients with nondesert IP (Figure 5b, $p = 0.83$).

DISCUSSION

In this study, we investigated various factors, including clinicopathological characteristics, immune cell infiltration, TIL density, and their relationship with survival outcomes in patients with TET who were treated with neoadjuvant therapy. First, our analysis revealed that more than 60% of the patients had immune-desert IP, whereas only 17.9% had

inflamed IP. No significant differences were observed between patients with desert and nondesert IP in terms of demographics and disease characteristics. However, the nondesert IP group showed a higher proportion of patients with a PR to neoadjuvant therapy in comparison to the desert IP group (63.6% vs. 17.6%, respectively; $p = 0.038$). Univariable and multivariable analyses confirmed that desert IP of the pre-neoadjuvant specimen was associated with a higher likelihood of PR to neoadjuvant therapy. Second, we confirmed that both iTIL and sTIL densities increased after neoadjuvant therapy. In addition, higher iTIL and sTIL were associated with longer OS. Although the cutoff value needs to be further studied due to the small number of patients included in our study, the higher iTIL group with cutoff value determined by OS analysis also had a longer DFS.

As complete resection is the most important prognostic factor for locally advanced, unresectable TET, downstaging with neoadjuvant therapy has been previously evaluated.^{13,21,22} However, despite the importance of the response to neoadjuvant therapy, predictive biomarkers are scarce. The only

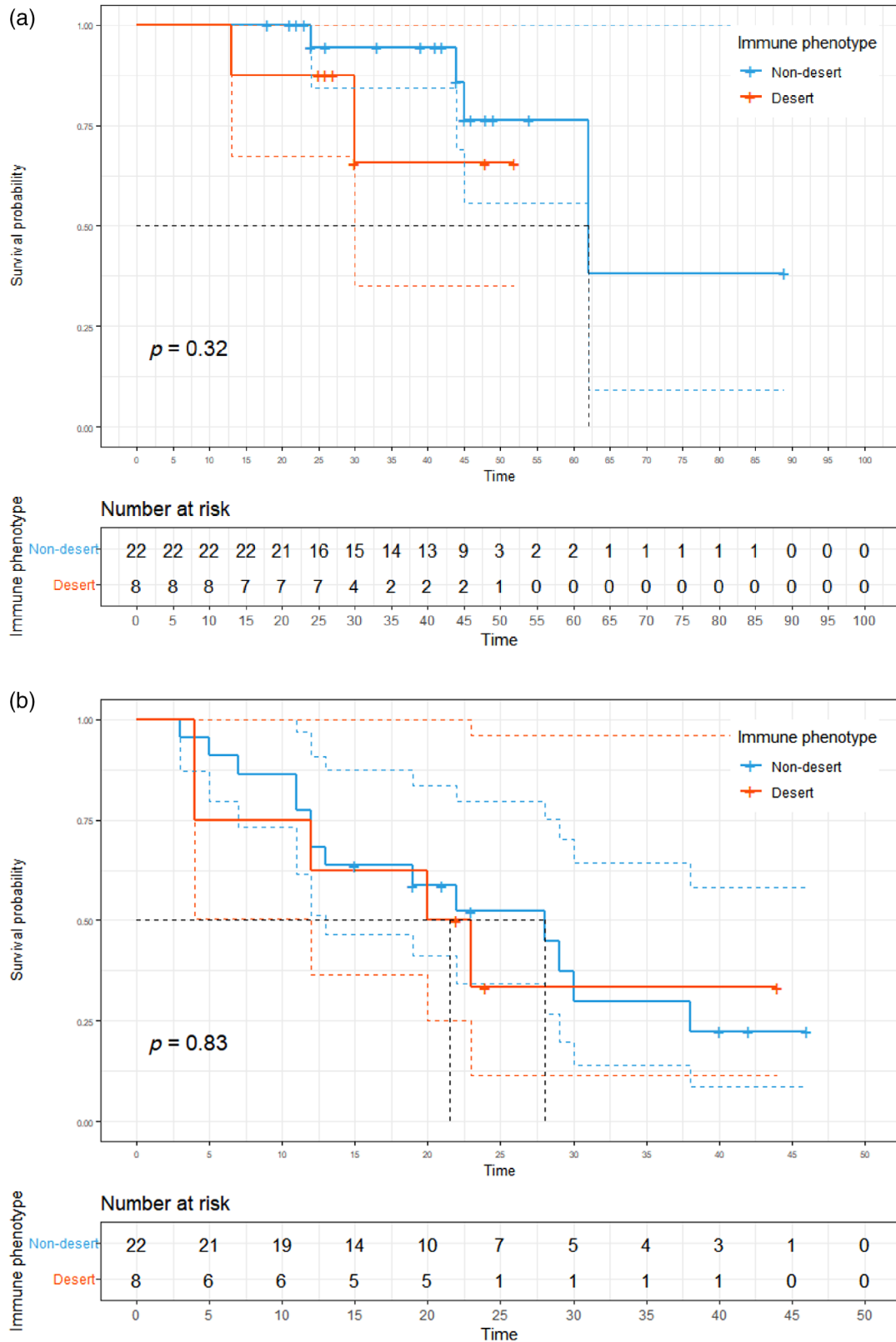


FIGURE 5 Survival outcomes based on immune phenotype. (a) Kaplan–Meier curves of overall survival (OS) based on immune phenotype. (b) Kaplan–Meier curves of disease-free survival (DFS) based on immune phenotype.

reported association is that it tends to be associated with high-risk histological types and greater response.¹³ Several attempts have been made to predict the response in patients with locally

advanced breast cancer, where neoadjuvant therapy is crucial such as TET,²³ and higher TIL levels in preneoadjuvant therapy biopsies have been reported to be associated with higher

rates of pCR.^{24–26} As TET is a rare cancer and pCR is rare in TET,^{13,21,22} finding a predictive biomarker for pCR was an arduous task. Instead, we found that preneoadjuvant IP, represented by spatial distribution of TIL, was associated with response to neoadjuvant therapy.

As TET is a highly heterogeneous group of diseases with a wide range of biological features and prognoses, there has been an ongoing effort to identify prognostic factors.^{27,28} Ever since genetic aberrations, including GTF2I mutation, have been reported in TET,^{29,30} several studies have investigated the genetic alterations and prognosis of TET.^{31,32} A previous study reported that classification by GTF2I mutation was associated with DFS and OS.³³ It has also been reported that classification of the tumor microenvironment by RNA sequencing is relevant to the prognosis of TET.³⁴

The present study demonstrated the usefulness of TIL density analyzed using Lunit SCOPE IO, an AI-powered spatial TIL analyzer, as a prognostic biomarker that would aid in determining the course of treatment after surgery followed by neoadjuvant therapy in patients initially diagnosed with unresectable TET. As an imaging biomarker that can be performed in a short time without additional techniques, such as staining or genetic analysis, we believe that TIL density analyzed by Lunit SCOPE IO would be useful and practical in clinical settings. Two phase 2 trials have evaluated the efficacy of pembrolizumab, an immune checkpoint inhibitor (ICI), in patients with refractory or recurrent TETs, and both confirmed the association of high PD-L1 with the response.^{35,36} Given the mechanism of action of ICIs, TIL density may also be a predictive biomarker of the use of ICIs in recurrent TETs. Future studies using multiple agents, including ICI or receptor tyrosine kinase inhibitors, in other clinical circumstances of TETs, besides neoadjuvant therapy, are warranted.

A major limitation of the present study was its small sample size and heterogeneous patient population. However, we believe that the small number of patients does not eliminate the significance of our study, considering the rarity of TET and the paucity of studies on TIL as biomarker in TET. Another limitation was the heterogeneity of the treatment modalities. Although the treatment was administered at a single institution, there may have been bias because the treatment course was determined by a multidisciplinary team. In addition, the AI-powered L-unit SCOPE IO has not yet been validated for TET. Although it has been validated in multiple cancer types, further validation in TET is required.

Despite these limitations, our study is the first to identify TIL levels as predictive and prognostic biomarkers using an AI-powered model in patients with TET. Although distinguishing between tumor cells of TET and TIL can be difficult, given that tumor cells in TET are of T cell origin, AI-based IP was able to make this distinction.²⁸ In addition, the findings in this study suggest that neoadjuvant therapy can lead to an increase in TIL density and a shift from immune desert to inflamed IP. These

findings provide valuable insights into the role of neoadjuvant therapy and immune microenvironment in TETs.

In conclusion, to the best of our knowledge, this is the first study to investigate TIL density as a biomarker using an AI-powered model in patients with TETs. Tumor IP analyzed using the Lunit SCOPE IO can be used as a predictive biomarker for neoadjuvant therapy in patients initially diagnosed with unresectable TET. Patients with higher iTIL ($>147/\text{mm}^2$) or sTIL density ($>232.1/\text{mm}^2$) had longer OS. Further studies with larger number of patients are warranted to validate the value of AI-powered spatial analysis of TIL as biomarker of TET.

AUTHOR CONTRIBUTIONS

Dong Hyun Kim: Data curation, formal analysis, writing-original draft.

Yoojoo Lim, Sukjun Kim, Chan-Young Ock: Formal analysis, methodology, writing-original draft.

Bhumsuk Keam: Conceptualization, funding acquisition, supervision.

All authors contributed to editing the final proof (writing-review and editing).

ACKNOWLEDGMENTS

This study was funded through a generous donation from Ms Soon-Hee Park. Despite losing her son to thymic carcinoma, she donated to support the progress of thymic carcinoma treatment. We are deeply grateful for her invaluable support.

CONFLICT OF INTEREST STATEMENT

BK received research funding from MSD, AstraZeneca, and Ono Pharmaceutical Co., Ltd., and has served as an advisor for Handok, NeoImmuneTec, Trialinformatics and ImmuneOncia outside of the current work. YL, KS, and C-YO are employees of Lunit, Inc., and own stocks and/or stock options of Lunit Inc. TMK has consulting or advisory roles in Amgen, AstraZeneca/MedImmune, Bayer, Boryung, Hanmi, IMBDx, Inc., Janssen, Novartis, Regeneron, Roche/Genentech, Samsung Bioepis, Sanofi, and Takeda. D-WK received research funding from Alpha Biopharma, Amgen, AstraZeneca/Medimmune, Boehringer-Ingelheim, Bridge BioTherapeutics, Chong Keun Dang, Daiichi-Sankyo, GSK, Hanmi, InnoN, Janssen, Merck, Merus, Mirati Therapeutics, MSD, Novartis, ONO Pharmaceutical, Pfizer, Roche/Genentech, Takeda, TP Therapeutics, Xcovery, Yuhan. KJN is a cofounder and chief medical officer of Portrai, Inc. CHK is an educational proctor of intuitive surgical Korea.

DATA AVAILABILITY STATEMENT

The datasets generated during the current study are available from the corresponding author on reasonable request.

ORCID

Dong Hyun Kim  <https://orcid.org/0000-0002-0369-5763>

Dong-Wan Kim  <https://orcid.org/0000-0001-5124-7132>

Hak Jae Kim  <https://orcid.org/0000-0003-3602-2263>

Bhumsuk Keam  <https://orcid.org/0000-0001-8196-4247>

REFERENCES

- Girard N, Ruffini E, Marx A, Faivre-Finn C, Peters S. Thymic epithelial tumours: ESMO clinical practice guidelines for diagnosis, treatment and follow-up. *Ann Oncol*. 2015;26:v40–55.
- Ahmad U, Yao X, Detterbeck F, Huang J, Antonicelli A, Filosso PL, et al. Thymic carcinoma outcomes and prognosis: results of an international analysis. *J Thorac Cardiovasc Surg*. 2015;149(1):95–101. e102.
- Kondo K, Monden Y. Therapy for thymic epithelial tumors: a clinical study of 1,320 patients from Japan. *Ann Thorac Surg*. 2003;76(3):878–84.
- Ichinose Y, Ohta M, Yano T, Yokoyama H, Asoh H, Hata K. Treatment of invasive thymoma with pleural dissemination. *J Surg Oncol*. 1993;54(3):180–3.
- Detterbeck FC, Parsons AM. Thymic tumors. *Ann Thorac Surg*. 2004;77(5):1860–9.
- National Comprehensive Cancer Network. Thymomas and Thymic Carcinomas, Version 1.2017. *NCCN Clinical Practice Guidelines in Oncology (NCCN Guidelines)*. 2017.
- Girard N, Mornex F, Van Houtte P, Cordier J-F, Van Schil P. Thymoma: a focus on current therapeutic management. *J Thorac Oncol*. 2009;4(1):119–26.
- Falkson CB, Bezjak A, Darling G, Gregg R, Malthaner R, Maziak DE, et al. The management of thymoma: a systematic review and practice guideline. *J Thorac Oncol*. 2009;4(7):911–9.
- Girard N, Lal R, Wakelee H, Riely GJ, Loehrer PJ. Chemotherapy definitions and policies for thymic malignancies. *J Thorac Oncol*. 2011;6(7):S1749–55.
- Macchiarini P, Chella A, Ducci F, Rossi B, Testi C, Bevilacqua G, et al. Neoadjuvant chemotherapy, surgery, and postoperative radiation therapy for invasive thymoma. *Cancer*. 1991;68(4):706–13.
- Rea F, Sartori F, Loy M, Calabrò F, Fornasiero A, Daniele O, et al. Chemotherapy and operation for invasive thymoma. *J Thorac Cardiovasc Surg*. 1993;106(3):543–9.
- Onuki T, Ishikawa S, Yamamoto T, Ito H, Sakai M, Onizuka M, et al. Pathologic radioresponse of preoperatively irradiated invasive thymomas. *J Thorac Oncol*. 2008;3(3):270–6.
- Korst RJ, Bezjak A, Blackmon S, Choi N, Fidias P, Liu G, et al. Neoadjuvant chemoradiotherapy for locally advanced thymic tumors: a phase II, multi-institutional clinical trial. *J Thorac Cardiovasc Surg*. 2014;147(1):36–46. e31.
- Engels EA, Pfeiffer RM. Malignant thymoma in the United States: demographic patterns in incidence and associations with subsequent malignancies. *Int J Cancer*. 2003;105(4):546–51.
- Park S, Ock C-Y, Kim H, Pereira S, Park S, Ma M, et al. Artificial intelligence-powered spatial analysis of tumor-infiltrating lymphocytes as complementary biomarker for immune checkpoint inhibition in non-small-cell lung cancer. *J Clin Oncol*. 2022;40(17):1916–28.
- Eisenhauer EA, Therasse P, Bogaerts J, Schwartz LH, Sargent D, Ford R, et al. New response evaluation criteria in solid tumours: revised RECIST guideline (version 1.1). *Eur J Cancer*. 2009;45(2):228–47.
- Johnson GB, Aubry MC, Eunhee SY, Koo CW, Jenkins SM, Garces YI, et al. Radiologic response to neoadjuvant treatment predicts histologic response in thymic epithelial tumors. *J Thorac Oncol*. 2017;12(2):354–67.
- Mandard AM, Dalibard F, Mandard JC, Marnay J, Henry-Amar M, Petiot JF, et al. Pathologic assessment of tumor regression after preoperative chemoradiotherapy of esophageal carcinoma. Clinicopathologic correlations. *Cancer*. 1994;73(11):2680–6.
- Ayers M, Lunceford J, Nebozhyn M, Murphy E, Loboda A, Kaufman DR, et al. IFN- γ -related mRNA profile predicts clinical response to PD-1 blockade. *J Clin Invest*. 2017;127(8):2930–40.
- Chen DS, Mellman I. Elements of cancer immunity and the cancer-immune set point. *Nature*. 2017;541(7637):321–30.
- Kim ES, Putnam JB, Komaki R, Walsh GL, Ro JY, Shin HJ, et al. Phase II study of a multidisciplinary approach with induction chemotherapy, followed by surgical resection, radiation therapy, and consolidation chemotherapy for unresectable malignant thymomas. *Lung Cancer*. 2004;44(3):369–79.
- Kunitoh H, Tamura T, Shibata T, Takeda K, Katakami N, Nakagawa K, et al. A phase II trial of dose-dense chemotherapy, followed by surgical resection and/or thoracic radiotherapy, in locally advanced thymoma: report of a Japan clinical oncology group trial (JCOG 9606). *Br J Cancer*. 2010;103(1):6–11.
- Loi S. The ESMO clinical practice guidelines for early breast cancer: diagnosis, treatment and follow-up: on the winding road to personalized medicine. *Ann Oncol*. 2019;30(8):1183–4.
- Solinas C, Ceppi M, Lambertini M, Scartozzi M, Buisseret L, Garaud S, et al. Tumor-infiltrating lymphocytes in patients with HER2-positive breast cancer treated with neoadjuvant chemotherapy plus trastuzumab, lapatinib or their combination: a meta-analysis of randomized controlled trials. *Cancer Treat Rev*. 2017;57:8–15.
- Denkert C, Loibl S, Noske A, Roller M, Müller BM, Komor M, et al. Tumor-associated lymphocytes as an independent predictor of response to neoadjuvant chemotherapy in breast cancer. *J Clin Oncol*. 2010;28(1):105–13.
- Van Bockstal MR, François A, Altinay S, et al. Interobserver variability in the assessment of stromal tumor-infiltrating lymphocytes (sTILs) in triple-negative invasive breast carcinoma influences the association with pathological complete response: the IVITA study. *Mod Pathol*. 2021;34(12):2130–40.
- Kadouri N, Nevo S, Goldfarb Y, Abramson J. Thymic epithelial cell heterogeneity: TEC by TEC. *Nat Rev Immunol*. 2020;20(4):239–53.
- Oramas DM, Moran CA. Thymoma: histologically a heterogeneous group of tumors. Paper presented at: Seminars in Diagnostic Pathology. 2022.
- Lee GY, Yang WI, Jeung HC, Kim SC, Seo MY, Park CH, et al. Genome-wide genetic aberrations of thymoma using cDNA microarray based comparative genomic hybridization. *BMC Genomics*. 2007;8(1):1–15.
- Petrini I, Meltzer PS, Kim I-K, Lucchi M, Park KS, Fontanini G, et al. A specific missense mutation in GTF2I occurs at high frequency in thymic epithelial tumors. *Nat Genet*. 2014;46(8):844–9.
- Radovich M, Pickering CR, Felau I, Ha G, Zhang H, Jo H, et al. The integrated genomic landscape of thymic epithelial tumors. *Cancer cell*. 2018;33(2):244–258.e210.
- Xin Z, Lin M, Hao Z, Chen D, Chen Y, Chen X, et al. The immune landscape of human thymic epithelial tumors. *Nat Commun*. 2022;13(1):5463.
- Lee H-S, Jang H-J, Shah R, Yoon D, Hamaji M, Wald O, et al. Genomic analysis of thymic epithelial tumors identifies novel subtypes associated with distinct clinical features molecular subtyping of thymic epithelial tumors. *Clin Cancer Res*. 2017;23(16):4855–64.
- Hou X, Lin S, Liu Y, Wang K, Yu Z, Jia J, et al. Analysis of the tumor microenvironment and mutation burden identifies prognostic features in thymic epithelial tumors. *Am J Cancer Res*. 2022;12(5):2387–96.
- Giaccone G, Kim C, Thompson J, McGuire C, Kallakury B, Chahine JJ, et al. Pembrolizumab in patients with thymic carcinoma: a single-arm, single-centre, phase 2 study. *Lancet Oncol*. 2018;19(3):347–55.
- Cho J, Kim HS, Ku BM, Choi YL, Cristescu R, Han J, et al. Pembrolizumab for patients with refractory or relapsed thymic epithelial tumor: an open-label phase II trial. *J Clin Oncol*. 2019;37(24):2162–70.

How to cite this article: Kim DH, Lim Y, Kim S, Ock C-Y, Youk J, Kim M, et al. Artificial intelligence-powered spatial analysis of tumor-infiltrating lymphocytes as a biomarker in locally advanced unresectable thymic epithelial neoplasm: A single-center, retrospective, longitudinal cohort study. *Thorac Cancer*. 2023;14(30):3001–11. <https://doi.org/10.1111/1759-7714.15089>